ELSEVIER

Journal of Molecular Structure: THEOCHEM 847 (2007) 32–38

THEO CHEM

www.elsevier.com/locate/theochem

The regiospecific synthesis of 8-bromocamphor revisited – A DFT computational study

Ingrid T. Sabbagh, Perry T. Kaye *

Department of Chemistry, Rhodes University, Grahamstown 6140, South Africa

Received 25 January 2007; received in revised form 28 August 2007; accepted 28 August 2007
Available online 7 September 2007

Abstract

Access to 8-bromocamphor, a critical intermediate in the proposed synthesis of multidentate, camphor-derived ligands for the construction of novel metathesis catalysts, requires regioselective bromination of D-(+)-camphor. A computational study, using the Accelrys DFT code, DMol^3, has provided new insights into the factors that appear to control the regioselective formation of 8-bromocamphor.

Keywords: Regioselective bromination; Camphor; DFT calculations

1. Introduction

There has been considerable interest in the application of metathesis in organic synthesis [1]. Various metathesis catalysts have been developed, notable examples being the Hoveyda [2] and the 1st- and 2nd-generation Grubbs-type catalysts [3,4]. Our ongoing interest in development of novel metathesis catalysts [5] and in the use of camphor derivatives in asymmetric synthesis [6] prompted us to explore the use of camphor-derived systems as multidentate ligands for the construction of ruthenium complexes as novel metathesis catalysts. More specifically, we have targeted the D-(+)-camphor (**1**)-derived, tridentate ligand **2** in the expectation that coordination with ruthenium will afford a chelated analogue **4** of the 1st-generation Grubbs-type catalyst **3** – an analogue in which carboxylate moieties replace the *trans*-equatorial chloride ligands. In this paper, we now discuss the results of a DFT-based study of the factors favouring selective formation of 8-bromocamphor (**5**; Scheme 1).

2. Computational methods

Density functional calculations were conducted using the Accelrys DMol^3 DFT code in MaterialsStudio (version 2.2)[7] on LINUX-based Pentium IV PC's. All calculations involved use of the generalized gradient approximation (GGA) functional by Perdew and Wang (PW91)[8] and the 'double numerical plus polarization' (DNP) basis set – a polarized split valence basis set of numeric atomic functions which are exact solutions to the Kohn–Sham equations for the atoms [9]. Convergence criteria for geometry optimizations were the default threshold values provided as Supplementary information. All calculations employed a method based on Pulay's [10] direct inversion of iterative subspace (DIIS) technique to accelerate SCF convergence using, where necessary, a small electron thermal smearing value of 0.005 Ha. Rotameric options were initially explored at the molecular mechanics level using the PC Spartan-Pro [11] software package and the MMFF force-field; rotamers were then subjected to DFT calculations using DMol^3.

Preliminary transition state geometries were obtained using the integrated linear synchronous transit/quadratic synchronous transit (LST/QST) method [12], and then subjected to full TS optimization using an eigenvector

* Corresponding author. Tel.: +27 46 6038254; fax: +27 46 6225109.
E-mail address: P.Kaye@ru.ac.za (P.T. Kaye).

0166-1280/$ - see front matter © 2007 Elsevier B.V. All rights reserved.
doi:10.1016/j.theochem.2007.08.033

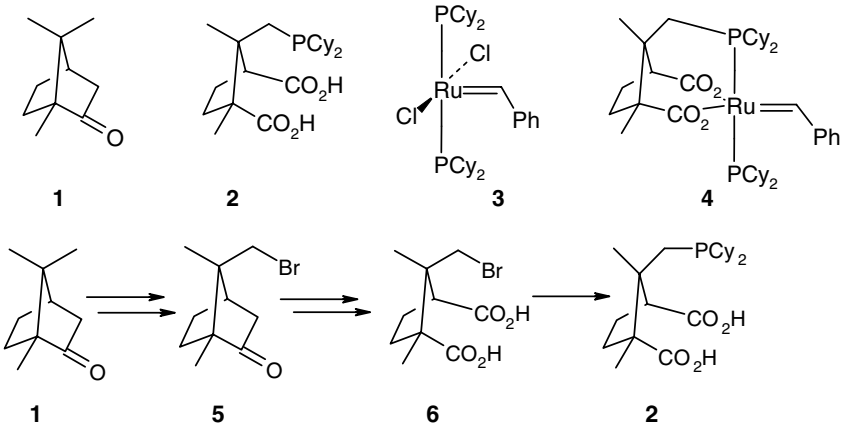

Scheme 1.

following algorithm. Where necessary, these geometries were confirmed using intrinsic reaction path (IRP) calculations, based on the nudged elastic band (NEB) algorithm [13], to map the pathways connecting the relevant reactant, transition state and product geometries. All structures identified as stationary points were subjected to frequency analysis, to verify their classification as equilibrium geometries (zero imaginary frequencies) or transition states (one imaginary frequency). The reported energies reflect Gibbs free energy corrections to the total electronic energies at 298.15 K and include zero-point energy (ZPE) corrections. Where indicated, solvent-corrected data were obtained from single-point calculations on geometry-optimized structures using the Conductor-like Screening Model (COSMO) [14] available in DMol^3 and a value of 60 for the dielectric constant of chlorosulfonic acid (60 ± 10), as determined by Gillespie and White [15].

3. Results and discussion

There appear to be relatively few examples of replacement of the chloride ligands in Grubbs-type systems; those that have been reported include the dimeric ruthenium carboxylates described by Mol and coworkers [16], and Grubbs' four-coordinate *tert*-butoxy catalyst [17]. Not only would the camphor-derived tridentate ligand **2** permit similar replacement of the chloride ligands, but several additional factors make research on its development attractive. Firstly, chelation of the ruthenium cation could stabilise the complex. Secondly, replacement of the *trans*-equatorial chloride ligands by carboxylate moieties would obviate the formation of chloride-bridged dimers which, it has been suggested, provide a decomposition pathway for Grubbs-type complexes [18]. Thirdly, functionalisation at C-9 or C-10 of the camphor system could provide a suitable anchor-point for immobilising the catalyst on a solid support and, fourthly, the well-established chemistry of camphor systems might be expected to provide reasonable synthetic access to the target ligand **2**. Finally, the inherent asymmetry of the targeted complex may offer a measure of stereocontol in catalytic applications. A Gibbs free energy (G_{298}) profile has been generated [19], using a truncated model, to explore the potential metathesis activity of complex **4** for the degenerate metathesis of ethylene; the results, which will be published in due course, appear to justify attempts to prepare the tridentate ligand **2**.

Access to the target molecule **2** was expected, in principle, to involve C-8 bromination of (+)-camphor **1**, subsequent oxidation to 8-bromocamphoric acid **6** and, finally, displacement of bromide by a dicyclohexylphosphine group (Scheme 1). In practice, the formation of the diacid **6** has proved to be problematic due to ready lactonisation, but (+)-8-bromocamphor **5**, the regiospecific formation of which is the subject of this paper, was successfully prepared from commercially available (+)-3-*endo*-bromocamphor **7** (Scheme 2), following the method reported by Money and coworkers [20–22]. Thus, 3,3-dibromocamphor **8**, obtained in 78% yield *via* solvent-free bromination of 3-*endo*-bromocamphor **7**, was subjected to bromination in chlorosulfonic acid to yield 3,3,8-tribromocamphor **9**. Debromination, using zinc in glacial acetic acid, then afforded 8-bromocamphor **5** in 33% overall yield from

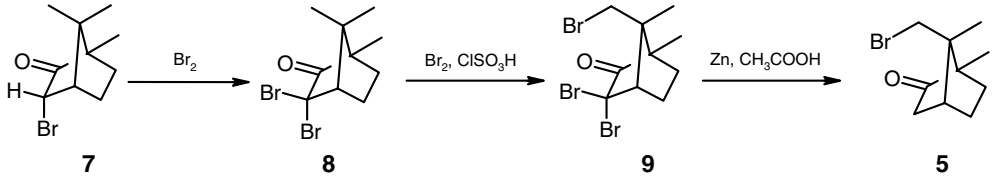

Scheme 2.

3-bromocamphor **8** (which is comparable to Money's [22] optimised yields of 30–40%) (Scheme 2).

The generally accepted mechanisms involved in the regiospecific formation of 8-bromocamphor **5** and the isomeric 9-bromocamphor **16** are consolidated in Scheme 3. The key steps determining selective formation of each of the isomeric products **5** and **16** involve a 2,3-*endo*-methyl shift (**13b** → **17**) and a 2,3-*exo*-methyl shift (**13a** → **14a**), respectively [21]. Money postulated that the energetically unfavourable 2,3-*endo*-methyl shift (**13b** → **17**) required the presence of a bulky substituent at the 7-*syn* position (i.e., X = Br)[21], and demonstrated that 3,3-dibromocamphor **8** could indeed be converted to 8-bromocamphor **5**. The mechanism proposed by Money is supported by the results of a ^{1}H NMR study [23] using deuterium-labelled precursors. However, the assumption that the 2,3-*endo*-methyl shift (**13b** → **17**) only occurs because the corresponding 2,3-*exo*-methyl shift (**13b** → **14b**) is inhibited by the bulky 7-*syn*-bromine substituent has been challenged by Antkowiak and Antkowiak [24], who attribute the observed 2,3-*endo*-methyl shift (**13b** → **17**) to anchimeric assistance by the 7-*syn* bromine atom, as illustrated in Fig. 1.

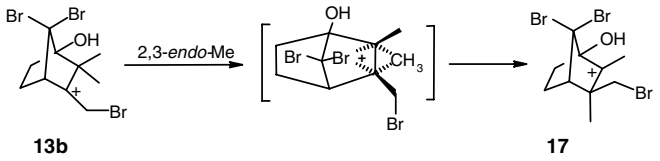

Fig. 1. Promotion of the 2,3-*endo*-methyl shift (**13b** → **17**) by anchimeric assistance as suggested by Antkowiak and Antkowiak [24].

Given the critical role of the 8-brominated product **5** as an intermediate in the proposed synthesis of the tridentate ligand **2** (Scheme 1), a computational study was undertaken to explore the mechanistic details of the transformations **13b** → **17** → **18** (Scheme 3). All relevant intermediates and associated transition states were optimised at the DFT level for the 8-bromination pathway, and the results are summarised in Table 1 and in Figs. 2–4. Since the reaction is conducted in chlorosulfonic acid, the carbonyl precursors **7** and **8** were viewed as the corresponding protonated analogues **10a** and **10b**.

Formation of the C-8 brominated product **5** (i.e., **13b** → **5**; Scheme 3) is complicated by the apparent competition between two rotamers of the intermediate **17**, arising from internal rotation about the CH_3C–CH_2Br bond axis. Although the rotational barrier is hardly significant ($\Delta G^{\ddagger}_{298} = 1.17$ kcal mol^{-1}, the computational data indicate these rotamers to be geometrically distinct equilibrium structures, separated by a transition state situated along the rotational coordinate. The calculated free energies of activation ($\Delta G^{\ddagger}_{298}$) for the 2,3-*endo*-methyl shifts associated with either rotamer [**13b** → **17i** (13.42 kcal mol^{-1}) or **13b** → **17ii** (11.54 kcal mol^{-1}; Fig. 2)] are relatively large, and provide an opportunity for less energy-demanding reactions to compete with the formation of the desired 8-bromocamphor **5**.

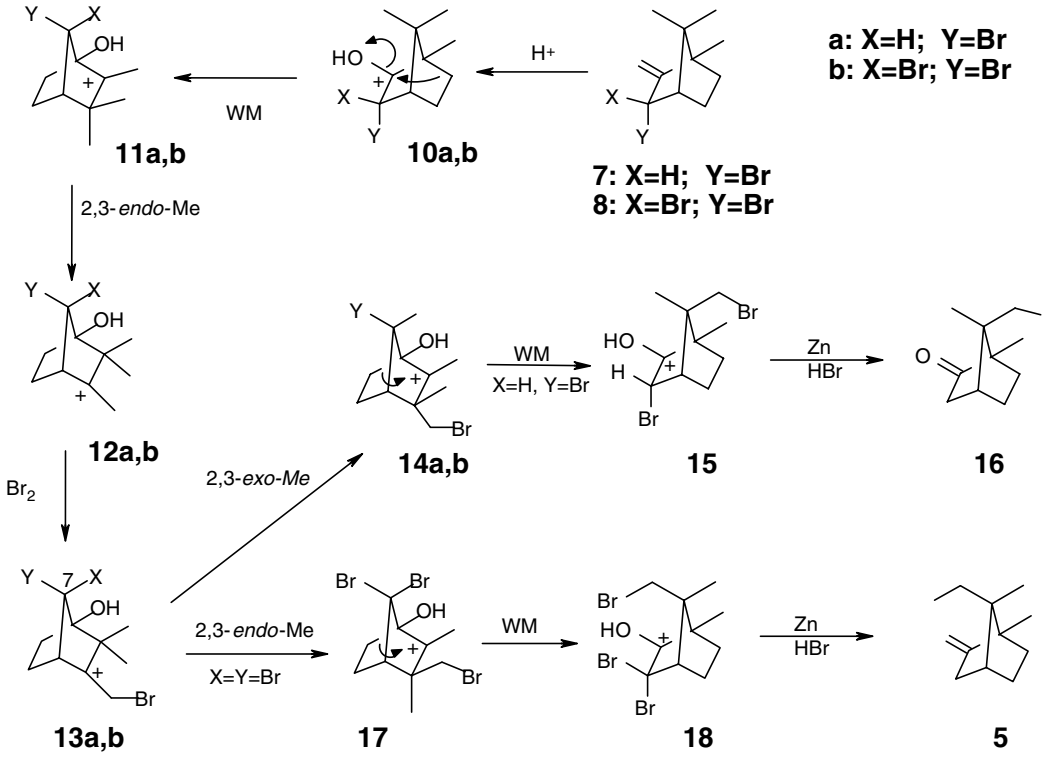

Scheme 3. Consolidated mechanistic sequence leading to 8-bromocamphor **5** and 9-bromo-camphor **16** (WM = Wagner–Meerwein rearrangement).

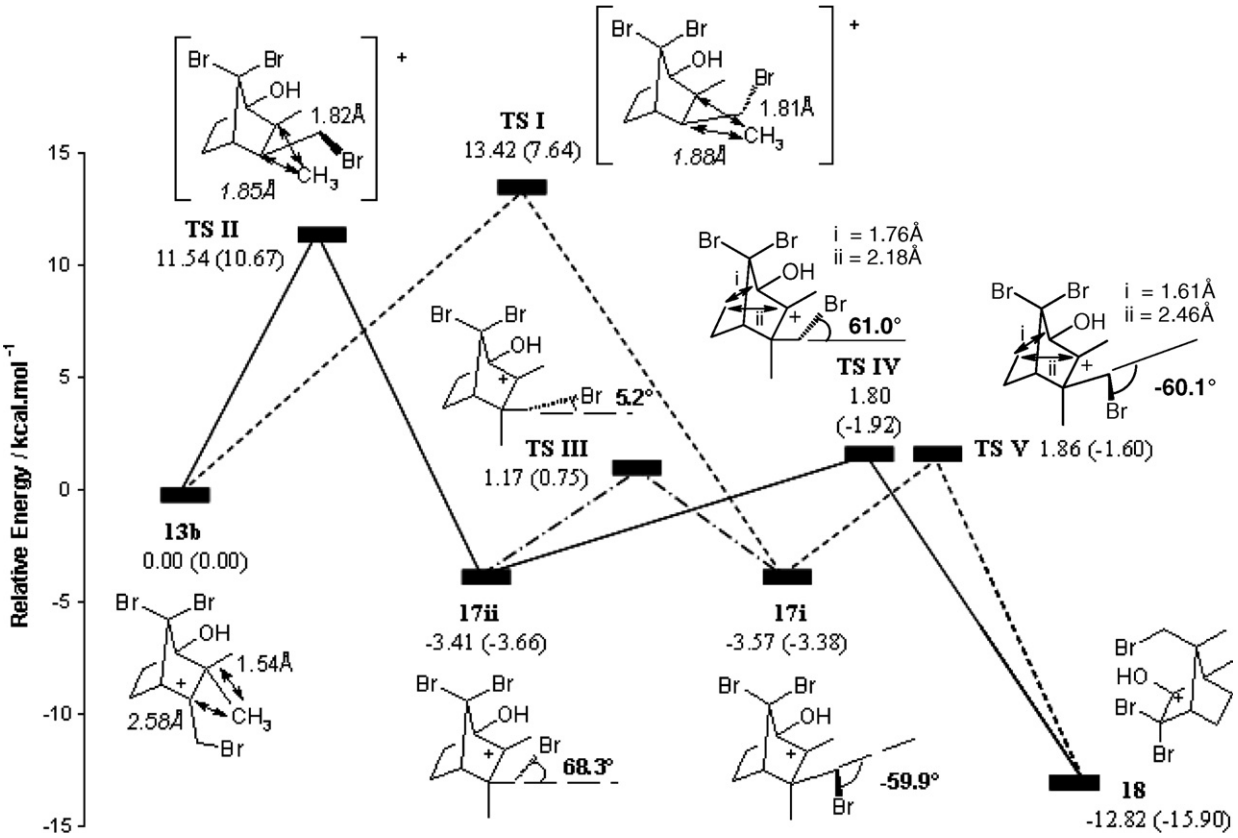

Fig. 2. Free energy diagram for pathway **13b** → **18** (X = Y = Br; Scheme 3), showing changing bond lengths (Å); italicised values refer to bonds formed in the 2,3-*endo*-methyl shift. The gas-phase free-energies are followed, in parentheses, by the solvent-corrected values. The torsion angles refer to the angles between Br and the CH_3 group on the adjacent carbon.

Table 1
DFT reaction energies (kcal mol^{-1}) for rearrangements of intermediate **13b** (X = Y = Br) outlined in Scheme 3, followed, in parentheses, by the solvent-corrected values

Reaction	ΔE	E_a	ΔG_{298}	$\Delta G^{\ddagger}_{298}$
13b → **17ii**	−2.67 (−3.59)	11.33 (10.41)	−3.41 (−3.66)	11.54 (10.67)
17ii → **17i**	−0.97 (0.22)	4.84 (3.42)	−0.16 (0.29)	4.58 (4.41)
17i → **18**	−11.34 (− 14.09)	4.28 (1.8)	−9.26 (−12.52)	5.43 (1.78)
17ii → **18**	−10.37 (−13.87)	4.91 (1.82)	−9.42 (−12.23)	5.21 (5.58)
13b → **17i**	−1.70 (−3.37)	13.93 (7.97)	−3.57 (−3.38)	13.42 (7.64)

The computational data, which are summarised in Table 1 and illustrated in Fig. 2, indicate that formation of intermediate **18** may proceed *via* rotamer **17i** (*i.e.*, **13b** → **TSI** → **17i** → **TSV** → **18**), rotamer **17ii** (*i.e.* **13b** → **TSII** → **17ii** → **TSIV** → **18**) or *via* combinations of both pathways involving internal rotation between structures **17i** and **17ii** . Stabilisation of **TS II** relative to **TS I** (by *ca.* 2 kcal mol^{-1} in the gas phase) may be attributed to an electrostatic attraction (approaching anchimeric assistance?) between the proximal CH_2Br moiety and the incipient carbocation in the former case. The importance of solvation effects, however, is apparent in the solvent-corrected data, which indicate **TSI** to be 3 kcal mol^{-1} more stable than **TSII**! In general, the solvent-corrected energies reflect net stabilization (relative to structure **13b**) of the structures examined, the only exception being the small increase (0.19 kcal mol^{-1}) in the relative free energy of cation **17i**.

The staggered rotameric options available to the precursor and rearranged carbocations **13b** and **18** (Fig. 2), respectively, were initially explored at the molecular mechanics level. At this level, only two stable rotamers were found for carbocation **13**, *viz.*, **13bi** and **13bii** (Fig. 3), while three stable rotamers were found for carbocation **18**. However, geometry optimisation at the DFT level permitted location of the three expected rotamers for each of the intermediates **13b** and **18**. The lowest energy rotamer **13bi** corresponds to structure **13b** as depicted in Fig. 2; the solvent-corrected energies, however, reflect a net stabilisation (−1.33 kcal mol^{-1}) of rotamer **13bii**. On the other hand, both gas-phase and solvent-corrected free energies clearly indicate **13biii** to be the least stable

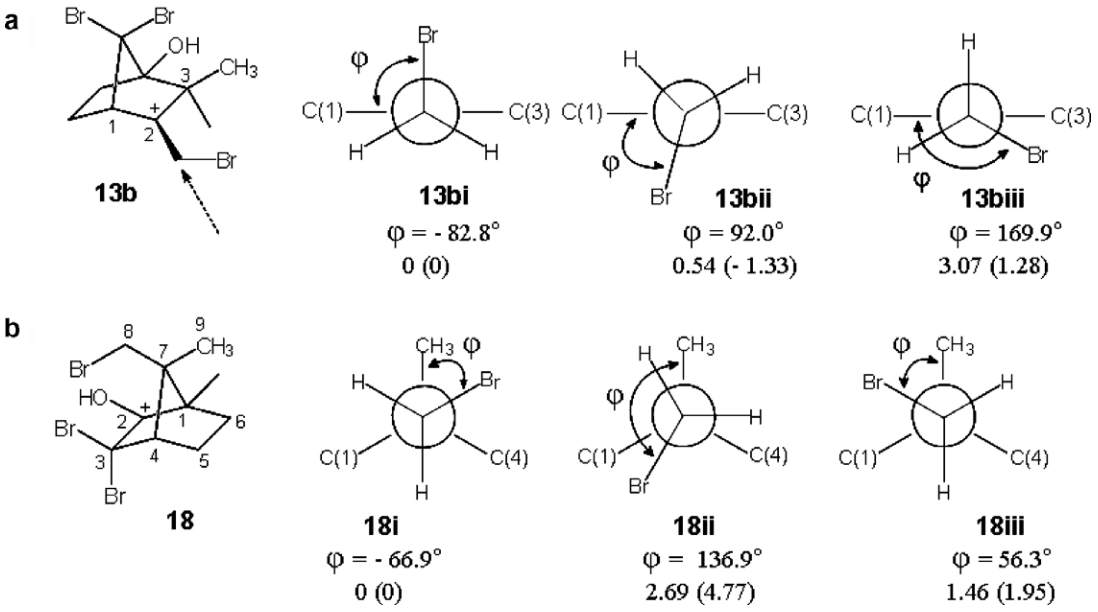

Fig. 3. Torsion angles (φ) and relative free energies (kcal mol^{-1}) for rotamers of: (a) the carbocation **13b**, viewed along the $BrCH_2$–C(2) bond axis; and (b) the rearranged carbocation **18**, viewed along the C(8)–C(7) bond axis. The gas-phase free-energies are followed, in parentheses, by the solvent-corrected values.

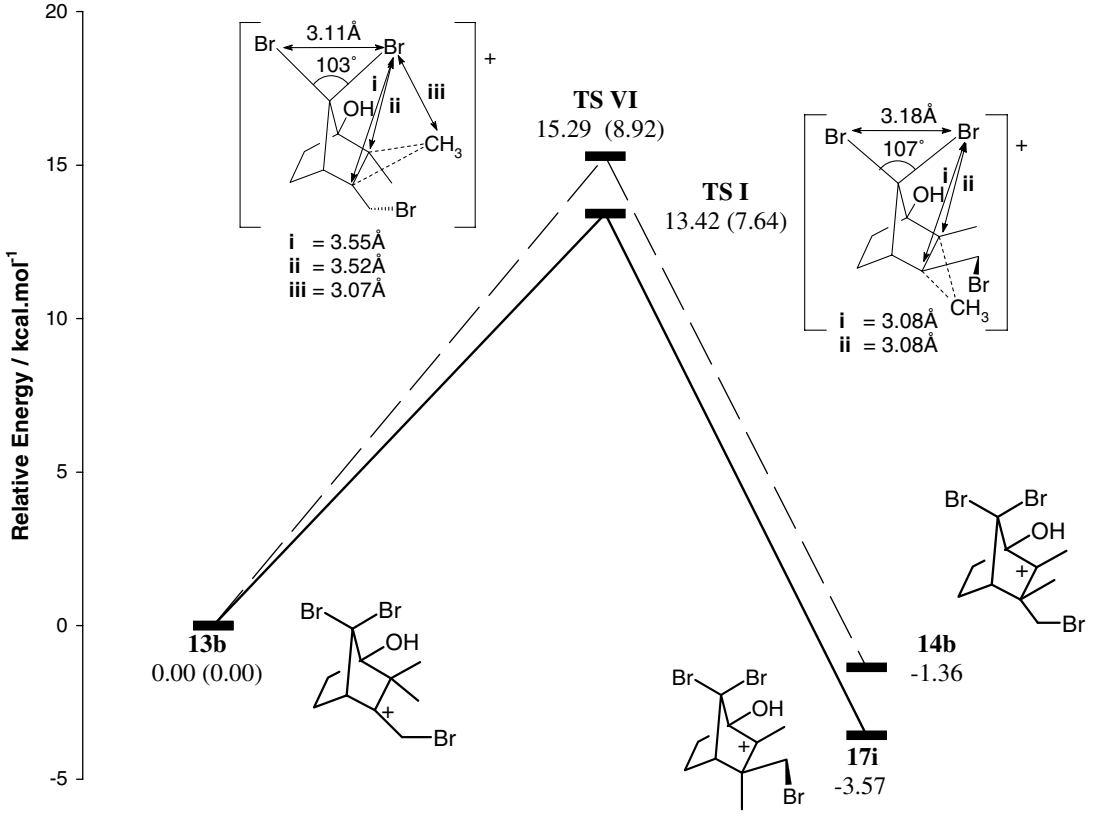

Fig. 4. Free energy diagram for pathways **13b** → **17i** and **13b** → **14b** (X = Y = Br; Scheme 3), showing changes in bond lengths (Å) and angles. The gas-phase free-energies are followed, in parentheses, by the solvent-corrected values.

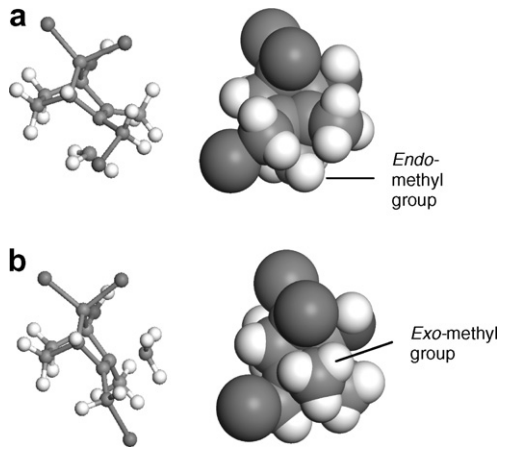

Fig. 5. Ball-and-stick and space-filling (rotated about the vertical axis to illustrate the steric effects; represented volumes are 77% of the van der Waals radii) models of transition state structures for: (a) the 2,3-*endo*-methyl shift (**TS I**); and (b) the 2,3-*exo*-methyl shift (**TS VI**) depicted in Fig. 4.

rotamer. In the case of the rearranged system **18**, the lowest energy rotamer **18i** corresponds to the structure depicted in Fig. 2. Interestingly, although the bonds approach an eclipsed arrangement in the least stable rotamer **18ii**, the structure appears to be stabilised by: intra-molecular hydrogen-bonding between the 8-bromo and 2-hydroxyl groups; relief of steric crowding between the 8-bromo and the proximate 3-*exo*-bromo atoms; or a combination of both effects. Of course, the rotational barriers between the rotamers are all low and, at room temperature, internal rotation is expected to be essentially unhindered.

In order to explore the observed preference exhibited by intermediate **13b** for a 2,3-*endo*- rather than a 2,3-*exo*-methyl shift, the free energies were determined for the respective transformations, **13b** → **17i** and **13b** → **14b**. The results are illustrated graphically in Fig. 4, from which it is apparent that the 2,3-*endo*-methyl shift (**13b** → **17i**) proceeds through a lower-energy transition state *and* affords the more stable rearranged carbocation **17i**.

Comparison of the transition states, **I** and **VI** (Fig. 4), provides interesting insights into the competing pathways. Thus, in the *endo*-transition state **TS I**, the distance between the 7-*syn*-bromine and the electron-deficient migration terminus, on one hand, and the migration origin, on the other (3.08 Å in *both cases*), is less than the sum of the van der Waals' radii (3.55 Å), indicating an electrostatic interaction consistent with the Antkowiaks' suggestion [24], that the 2,3-*endo*-methyl shift is facilitated by anchimeric assistance. In the case of transition state **VI**, however, the 7-*syn*-bromine and the migrating, nucleophilic *exo*-methyl group are only 3.07 Å apart. This separation is significantly less than the sum of the van der Waals' radii, indicating severe steric interaction – a conclusion supported by the apparent compression of the Br–C–Br angle (to 103° in **TS VI** compared to 107° in **TS I**). These results lend credence to Money's assumption that the 2,3-*exo*-methyl shift is inhibited by a bulky 7-*syn*-substituent [21]. The steric effects are illustrated graphically in Fig. 5.

It thus seems that the *anchimeric assistance* suggested by the Antkowiaks [24] and the *steric inhibition effect* assumed by Money [21] may well *operate in concert* to favour a 2,3-*endo*-methyl shift in the presence of the bulky 7-*syn*-bromine! However, comparison of the geometries of the intermediates **13a** and **13b** (Fig. 6) also reveals a significant torsional effect in **13b**, arising from the electrostatic attraction and consequent shortening of the distance between the electron-rich 7-*syn*-bromine and the cationic centre, C-2 (2.89 Å), compared to the corresponding distance to C-3 (3.23 Å). The resulting asymmetric twisting of the bicyclic skeleton influences, in turn, the dihedral angles **α**[C(3)–C(8)/C(2)–C(10)] and **β**[C(3)–C(9)/C(2)–C(10)] which, under "normal circumstances", would be expected to approximate to 60°. Since **β** is significantly larger than **α** in the tribromo intermediate **13b**: (i) the 9-*endo*-methyl-C(3) bond approaches an orientation parallel to the empty p-orbital at C-2 more closely than the 8-*exo*-methyl-C(3) bond, thus favouring migration of the former; and (ii) the smaller **α** angle means that the 8-*exo*-methyl group is closer to the position it will adopt following 9-*endo*-methyl migration. In the dibromo analogue **13a**, on the other hand, **α** > **β** – a situation, it might be argued, that would favour 8-*exo*-methyl migration; however, both dihedral angles may be sufficiently close to 60° to render any torsional contribution less significant. This argument is illustrated by the anticipated, relative orientations of the pertinent orbital axes for the respective intermediates

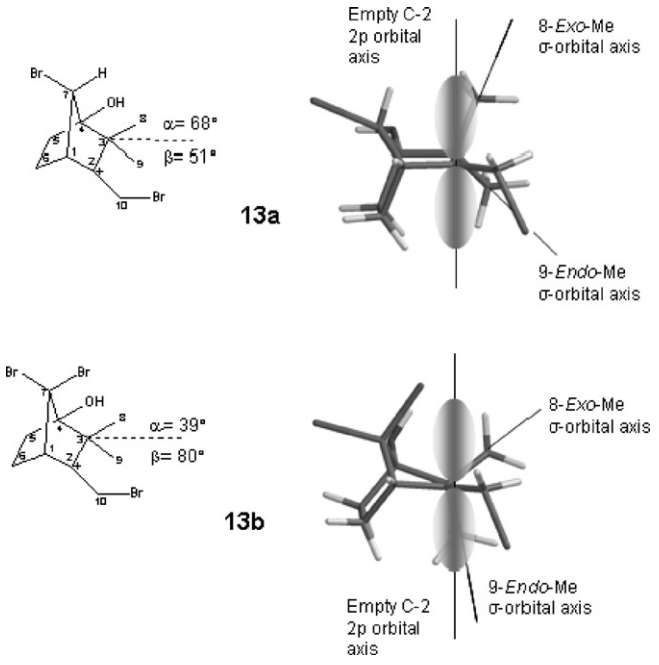

Fig. 6. Graphical representations of intermediates **13a** (X = Br, Y = H) and **13b** (X = Y = Br), showing dihedral angles (along the C(3)–C(2) bond axis) and potential overlap between the empty p-orbital on C-2 and the 8-*exo*-methyl- and 8-*endo*-methyl σ-orbitals in each case.

(Fig. 6). Thus, in the case of intermediate **13b**, in particular, the 9-*endo*-methyl-C(3) σ-orbital axis approaches co-planarity with the empty 2*p*-orbital at the migration terminus (C-2), whereas the 8-*exo*-methyl-C(3) σ-orbital axis is almost orthogonal. While Money [25] considered the possible involvement of torsional effects, he concluded, in the absence of experimental or computational evidence, that steric hindrance provided a more compelling explanation for 9-*endo*-methyl migration in the 7-bromo analogue **13b**. Interestingly, torsional factors have also been considered to influence similar migration in the racemization of camphene *via* a Nametkin rearrangement [26].

4. Conclusions

The results of this DFT study clearly provide theoretical support for the empirical steric inhibition and anchimeric assistance rationalisations used by Money [21] and the Antkowiaks [24], respectively, to account for the observed regioselectivity in the formation of 8- and 9-bromocamphor. In addition to these factors, however, it seems that torsional effects could also play a role in controlling selectivity. These mechanistic insights may prove useful in optimising selectivity in the rearrangement of camphor-derived systems, in general, and C-8 functionalisation of camphor, in particular.

Acknowledgements

The authors thank Sasol Technology Ltd. for a bursary (I.T.S) and Sasol Technology Ltd., the Technology and Human Resources for Industry Programme (THRIP; Project No. 2642) and Rhodes University for generous financial support, and the referee for constructive comments.

Appendix A. Supplementary data

Supplementary data associated with this article can be found, in the online version, at doi:10.1016/j.theochem.2007.08.033.

References

[1] K.J. Ivin, J. Mol. Catal. A: Chem 133 (1998) 1.
[2] J.S. Kingsbury, J.P.A. Harrity, P.J. Bonitatebus Jr., A.H. Hoveyda, J. Am. Chem. Soc. 121 (1999) 791.
[3] P. Schwab, R.H. Grubbs, J.W. Ziller, J. Am. Chem. Soc. 118 (1996) 100.
[4] M. Scholl, T.M. Trnka, J.P. Morgan, R.H. Grubbs, Tetrahedron Lett. 40 (1999) 2247.
[5] I.T. Sabbagh, P.T. Kaye, J. Mol. Struct.: THEOCHEM. 763 (2006) 37.
[6] See, for example P.T. Kaye, W.E. Molema, J. Chem. Soc. Chem. Commun. (1998) 2479.
[7] B. Delley, J. Chem. Phys. 92 (1990) 508;
B. Delley, J. Phys. Chem. 100 (1996) 6107;
B. Delley, J. Chem. Phys. 113 (2000) 7756.
[8] J.P. Perdew, Y. Wang, Phys. Rev. B45 (1992) 13244.
[9] W. Kohn, L.J. Sham, Phys. Rev. A140 (1965) 1133.
[10] P. Pulay, J. Comp. Chem. 3 (1982) 556.
[11] PC SPARTAN-Pro, version 1.1, Wavefunction, Inc., Irvine, 1999.
[12] T.A. Halgren, W.N. Lipscomb, Chem. Phys. Lett. 49 (1977) 225.
[13] G. Henkelman, H. Jonsson, J. Chem. Phys. 113 (2000) 9978.
[14] A. Klamt, G. Schueuermann, J. Chem. Soc. Perkin Trans. 2 (1993) 799.
[15] R.J. Gillespie, R.F.M. White, Trans. Faraday Soc. 54 (1958) 1846.
[16] W. Buchowicz, J.C. Mol, M. Lutz, A.L. Spek, J. Organomet. Chem. 588 (1999) 205;
W. Buchowitz, F. Ingold, J.C. Mol, M. Lutz, A.L. Spek, Chem. Eur. J. 7 (2001) 2842.
[17] M.S. Sanford, L.M. Henling, M.W. Day, R.H. Grubbs, Angew. Chem. Int. Ed. 39 (2000) 3451.
[18] D. Amoroso, G.P.A. Yap, D.E. Fogg, Organometallics 21 (2002) 3335.
[19] I.T. Sabbagh, PhD thesis, Rhodes University, Grahamstown, 2005.
[20] C.R. Eck, R.W. Mills, T. Money, J. Chem Soc. Chem. Commun. (1973) 911;
C.R. Eck, R.W. Mills, T. Money, J. Chem. Soc. Perkin Trans. 1 (1975) 251.
[21] P. Cachia, N. Darby, C.R. Eck, T. Money, J. Chem. Soc. Perkin Trans. 1 (1976) 359.
[22] J.H. Hutchinson, T. Money, S.E. Piper, Can. J. Chem. 64 (1986) 854.
[23] W.M. Dadson, T. Money, J. Chem Soc. Chem. Commun. (1982) 112.
[24] R. Antkowiak, W.Z. Antkowiak, Polish J. Chem. 68 (1994) 2297.
[25] W.M. Dadson, J.H. Hutchinson, T. Money, Can. J. Chem. 68 (1990) 1821.
[26] P.C. Moews, J.R. Knox, W.R. Vaughan, J. Am. Chem. Soc. 100 (1978) 260.